Journal of Molecular Liquids 294 (2019) 111656

Contents lists available at ScienceDirect

Journal of Molecular Liquids

journal homepage: www.elsevier.com/locate/molliq

Influence of molecular design on the morphology of nanoparticles formed from 1-alkyl-6-alkoxy-quinolinium cations and 4-sulfonatocalix[*n*]arenes

Véronique Wintgens [a], Zsombor Miskolczy [c], Jean-Michel Guigner [b], Catherine Amiel [a], László Biczók [c,*]

[a] Université Paris Est, ICMPE (UMR7182), CNRS, UPEC, F 94320 Thiais, France
[b] Institut de Minéralogie, de Physique des Matériaux et de Cosmochimie, IMPMC, Sorbonne Université, IRD, CNRS UMR 7590, MNHN, 4 Place Jussieu, 75005 Paris, France
[c] Institute of Materials and Environmental Chemistry, Research Centre for Natural Sciences, Hungarian Academy of Sciences, P.O. Box 286, 1519 Budapest, Hungary

ARTICLE INFO

Article history:
Received 8 July 2019
Received in revised form 24 August 2019
Accepted 27 August 2019
Available online 28 August 2019

Keywords:
Calorimetry
Nanostructure
Amphiphile
Self-assembly
Micelle

ABSTRACT

In order to reveal the influence of the guest molecular structure, the interactions between 4-sulfonatocalix[*n*]arene (SCXn) cavitands ($n = 4$ or 6) and two series of quinolinium derivatives were studied in neutral aqueous solutions at 298 K. For this, the long alkyl chain of the quinoliniums was attached either to the heterocyclic nitrogen ($C_mC_1OQ^+$ m = 10, 12, or 14) or to the oxygen located in position 6 of the aromatic system ($C_1C_mOQ^+$ m = 8, 10, or 12). All the quinolinium derivatives self-assembled with SCXn into nanoparticles (NP), whose size, zeta potential and composition were determined over a large molar mixing ratio range. Isothermal titration calorimetry showed that host-guest binding assisted the formation of negatively charged NPs in exothermic processes. The enthalpy gain in these associations significantly increased with the lengthening of the 1-alkyl group but was insensitive to the size of the SCXn macrocycle. The morphology of NPs was studied by cryo-TEM method. $C_mC_1OQ^+$ organization with SCXn led to spherical NPs without regular inner structure. In contrast, $C_1C_mOQ^+$-SCXn nanoaggregates usually had various shapes and the original morphologies exhibited lamellar domains with ~3 nm layer thickness. The different orientation of $C_mC_1OQ^+$ and $C_1C_mOQ^+$ in the cavitand was proposed to rationalize the morphological alterations.

1. Introduction

Host–guest binding of simple molecular building blocks is a powerful tool to mediate the formation of a wide variety of supramolecular architectures [1]. The most frequently used hosts are cyclodextrins, which are valuable constituents of nanoparticle-based drug carrier systems [2]. They can modulate the self-organization of amphiphiles, and their complexes with surfactants can produce various types of aggregates [3–5]. Confinement in cyclodextrin cavity was utilized for amphiphilicity adjustment of macromolecules, surface modification of nanoscale objects, and to create diverse nanoassemblies [6–9]. The length of the carbon chain and the degree of substitution significantly influenced the morphology and supramolecular structure of the nanoparticles fabricated from alkylated β-cyclodextrins [10].

4-Sulfonatocalix[*n*]arenes (SCXn) can be more advantageously applied as hosts than cyclodextrins in the construction of self-assembled systems. This is related to the polyanionic character, pH-sensitivity, larger solubility and conformational flexibility of the SCXn macrocycles. Additionally, their substantial binding affinity towards amphiphilic guests facilitate the further association into nanoparticles [11], vesicles [12–14], supramolecular micelles [15–17], or stimuli-responsive nanostructures [18–20]. A recent paper provides excellent overview on the advances in the recognition and assembly properties of this type of cavitands [21]. The structural motifs of SCXn complexes have been intensively examined in the solid state [22,23], but the relationship between the molecular structure of SCXn-containing supramolecular amphiphiles and the properties of their nanoparticles produced in solution is still not fully understood. It cannot be predicted how the characteristics of the constituents influence the size, shape and inner structure of the nanospecies created by spontaneous self-organization in water.

To find general trends, the main goal of the present studies was to reveal how the molecular structure variation affects the enthalpy of association and the morphology of the nanoparticles yielded by simple mixing of the components. We focused on the SCXn-induced aggregation of a new family of amphiphiles possessing a functionalized quinolinium head group. Two series of quinolinium derivatives were synthesized in which the long alkyl chain was attached either to the heterocyclic nitrogen ($C_mC_1OQ^+$ m = 10, 12, or 14) or to the oxygen located in position 6 of the aromatic system ($C_1C_mOQ^+$ m = 8, 10, or 12). Formulas of the employed compounds are presented in Scheme 1. Our previous study demonstrated that the homologues comprising

* Corresponding author.
E-mail address: biczok.laszlo@ttk.mta.hu (L. Biczók).

https://doi.org/10.1016/j.molliq.2019.111656

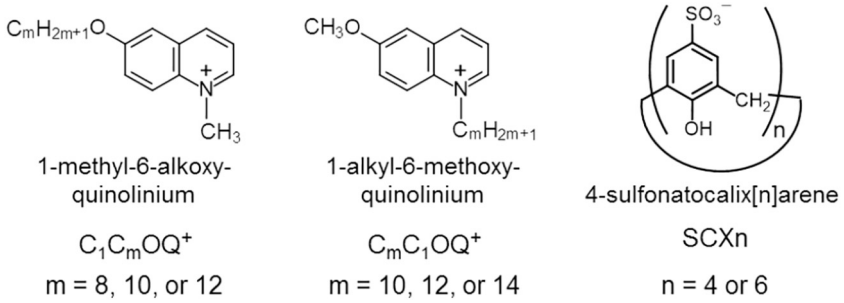

Scheme 1. Chemical structure of the components used in the present study

shorter aliphatic groups produced only 1:1 complexes with 4-sulfonatocalix[4 or 6]arenes in enthalpy driven processes and larger aggregates were not generated [24]. Additionally, NMR results showed different incorporations of the aliphatic group into SCX4: four carbons of the N-alkyl chain were located inside the macrocycle, while the alkoxy chain entirely protruded from the SCX4 cavity. Now, we intend to unravel how such kinds of differences alter the internal structure of self-assembled nanoparticles. The variation of the molecular structure of the constituents is an appealing way to tune the shape and internal geometric arrangements of nanosized aggregates. The control of not only the size but also the morphology of nano-objects would be highly beneficial in many potential applications. Hence, information on the relationship between chemical structure and the ordering of the building blocks in the course of self-organization is of crucial importance for the rational design of tailor-made nanoproducts.

2. Materials and methods

2.1. Materials

4-Sulfonatocalix[4]arene (SCX4) and 4-sulfonatocalix[6]arene (SCX6) were purchased from Acros Organics and used after drying under vacuum at 343 K overnight. Double distilled water served as solvent and the pH of the SCXn solutions was adjusted to 7 using the minimum volume of concentrated NaOH. The different 1-alkyl-6-alkoxy-quinolinium salts were synthesized and characterized by ^{1}H NMR spectroscopy as described in the Supporting Information. $C_mC_1OQ^+$ cations were used as Br^- salts, whereas $C_1C_mOQ^+$ homologues had I^- counterions. The preparation of 1-tetradecyl-6-methoxy-quinolium bromide ($C_{14}C_1OQ^+Br^-$) has been reported [17].

2.2. Sample preparation

Nanoparticles (NP) were generated by mixing the appropriate amounts of 2 mM or 4 mM 1-alkyl-6-alkoxy-quinolinium and 1 mM SCXn (pH 7) solutions under stirring at 150 rpm. Because of the low solubility, the 1 mM stock solutions of the $C_1C_{10}OQ^+I^-$ and $C_1C_{12}OQ^+I^-$ compounds were gentle heated before each use. SCXn concentration was kept constant (0.1 mM) unless otherwise noted. All experiments were conducted at neutral pH, where according to the reported deprotonation constants [25], SCX4 and SCX6 contained either one or two phenolate groups, leading to a 5-fold or 8-fold negatively charged SCX4 and SCX6 anions, respectively.

2.3. Instrumentation

^{1}H NMR spectra were recorded in deuterated DMSO on a Bruker Avance II 400 MHz NMR spectrometer. The absorption spectra were obtained on an Agilent Technologies Cary60 spectrophotometer. Particle size was determined by dynamic light scattering on a Zetasizer Nano-ZS (Malvern Instrument) equipped with a He—Ne laser ($\lambda = 633$ nm, scattering angle 173°) at 296 K. Each measurement was the average of 12 runs of 10 s. Data were analyzed with the software developed by the manufacturer using a distribution analysis (General Purpose analysis). The mean diameter of the NPs was calculated on the basis of number distribution. Experiments were repeated at least twice. NPs were separated from the liquid phase by an ultracentrifuge from Beckman Coulter (Optima Max-XP, type TLA 110 rotor). Total carbon analyses were performed on a Shimadzu TOC-L CSN instrument, which was calibrated by a potassium hydrogen phthalate solution in ultrapure water (2.125 g dm^{-3} corresponding to 1000 mgC dm^{-3}). ITC measurements were carried out with a MicroCal VP-ITC microcalorimeter at 298 K. Quinolinium solutions were injected from the computer controlled microsyringe at an interval of 180 s into the cell (volume = 1.4569 mL) containing 0.1 mM SCXn solution at pH 7, while stirring at 450 rpm. Cryogenic transmission electron microscopy images were taken on an UltraScan 2 k × 2 k CCD camera (Gatan, USA), using a LaB_6 JEOL JEM 2100 (JEOL, Japan) cryo-microscope operating at 200 kV with a JEOL low dose system (Minimum Dose System, MDS) to protect the thin ice film from any irradiation before imaging and to reduce the irradiation during the image capture. The images were recorded at 93 K and digitally corrected using the ImageJ software. The samples were prepared as previously reported [11].

3. Results

3.1. Micelle formation

Before the study of the association with SCXn, the enthalpy change upon dilution of 1-alkyl-6-methoxy-quinolium aqueous solutions was examined by isothermal titration calorimetry (ITC). The solubility of 1-methyl-6-alkoxy-quinolium iodides ($C_1C_mOQ^+I^-$) was low at 298 K. For example, it was lower than 4 mM for $C_1C_8OQ^+I^-$. The addition of close to saturated $C_1C_mOQ^+I^-$ solutions to water brought about negligible enthalpy variation indicating the insignificant ion association of these amphiphiles even at the highest concentration reached in water at 298 K. No micelles were formed at this temperature.

In contrast, larger solubility could be attained for 1-alkyl-6-methoxy-quinolium bromides ($C_mC_1OQ^+Br^-$). Fig. S1 presents the results of ITC experiments for the injection of 13.8, 14.8, and 88.6 mM solutions of tetradecyl, dodecyl-, and decyl homologues into water, respectively. Endothermic dilutions were always found and the enthalpograms demonstrated the association into micelles in the titrant solutions. In the initial stage of titration, the micelles fully dissociated because the concentration in the final solution remained below the critical micelle concentration (cmc). The small incipient increase of ΔH with concentration for $C_{12}C_1OQ^+Br^-$ and $C_{10}C_1OQ^+Br^-$ originated from the contribution of the electrostatic interactions among ions to the dilution heat [26]. The sharp diminution of ΔH implied that cmc was reached in the titrand solution and as a consequence, the heat evolution in this second concentration domain was due to the dilution of micellar solutions. The location of the inflexion point, which was determined from the minimum of the first derivative of the enthalpograms, corresponded to the cmc [27]. ITC measurements at 298 K provided

0.66 mM, 2.65 mM, and 11.6 mM values for the cmc of $C_{14}C_1OQ^+Br^-$, $C_{12}C_1OQ^+Br^-$, and $C_{10}C_1OQ^+Br^-$, respectively. The heat release upon dilution indicated that the association of these amphiphiles to micelles was enthalpically favored. The lengthening of the alkyl chain decreased the ΔH of micellization in the series of $\Delta H(C_{10}C_1OQ^+) = -5.7\ kJ\ mol^{-1} > \Delta H(C_{12}C_1OQ^+) = -7.4\ kJ\ mol^{-1} > \Delta H(C_{14}C_1OQ^+) = -11.9\ kJ\ mol^{-1}$.

3.2. Calorimetric study of the self-assembly with SCXn

To ensure that no micelle formation took place in the titrant solution, 1-alkyl-6-alkoxy-quinolinium concentration was always kept below the cmc in the course of ITC measurements of the self-organization with SCXn at 298 K. The enthalpograms were corrected by the dilution heat.

When SCX4 was titrated with $C_1C_8OQ^+$, the enthalpogram showed a peculiar shape (Fig. 1A). After the substantial incipient enthalpy (ΔH) release, |ΔH| reached a minimum at $[C_1C_8OQ^+]/[SCX4] = 1.4$ mixing ratio, and then, increased attaining a plateau. Upon further increase of $C_1C_8OQ^+$ concentration, |ΔH| gradually vanished in the $5.5 < [C_1C_8OQ^+]/[SCX4] < 8.0$ range. These trends indicate two major association processes. The initial enthalpy gain is attributed to complex formation because the first part of the experimental data can be fitted assuming 1:1 host-guest binding (Fig. 1B). The nonlinear least-squares analysis provided an association constant of K around $1.2 \times 10^5\ M^{-1}$, which agreed with the trend reported for the corresponding values of the 1:1 association between SCX4 and $C_1C_mOQ^+$ possessing a shorter aliphatic chain [24]. K varied from $4.5 \times 10^5\ M^{-1}$ to $3 \times 10^5\ M^{-1}$ when the number of carbon atoms in the alkyl substituent was changed from 1 to 6. Dynamic light scattering measurements demonstrated that nanoparticles (NP) were produced at $[C_1C_8OQ^+]/[SCX4] \geq 2$ mixing ratios (vide infra). Therefore, the almost constant enthalpy change in the $2.5 \leq [C_1C_8OQ^+]/[SCX4] \leq 5.5$ range is due to the association to NPs. These ITC results suggest that the 1:1 quinolinium-SCX4 complex formation is a prerequisite of the self-organization into NPs. The hydrophobic interaction among the aliphatic chains and the electrostatic attraction of the quinolinium head group to SCX4 promote NP production.

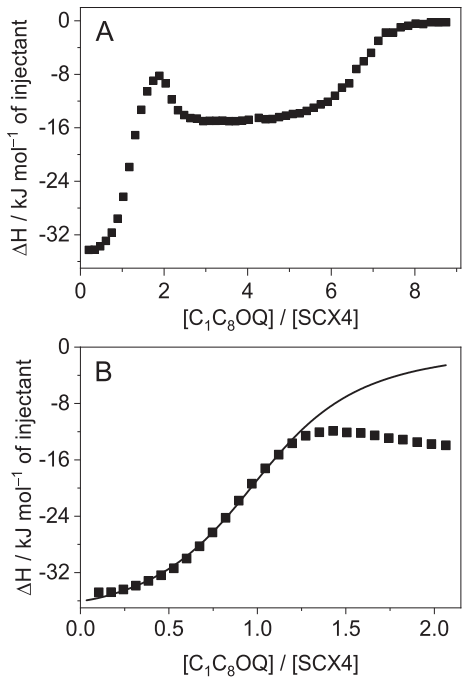

Fig. 1. (A) Integrated heat evolved per injection (obtained after subtraction of the dilution heat to raw data) for the titration of 0.1 mM SCX4 solution with 2 mM $C_1C_8OQ^+$. (B) The zoomed view of the enthalpogram at low $[C_1C_8OQ^+]/[SCX4]$ mixing ratios. The line represents the best fit of the initial part using the 1:1 complexation model.

The complex and NP formations are less separated when $C_1C_{10}OQ^+$ is added to SCX4 solution instead of $C_1C_8OQ^+$ (Fig. S2) because the increase of the aliphatic chain length leads to somewhat more exothermic self-organization into NPs at lower quinolinium concentration. The low solubility of $C_1C_{12}OQ^+$ did not allow calorimetric experiments, but NPs production was found (vide infra).

Fig. 2 presents the enthalpograms for the titration of SCX4 with various $C_mC_1OQ^+$ derivatives. The lengthening of the aliphatic chain linked to the heterocyclic nitrogen brought about similar behavior to that found for $C_1C_mOQ^+$. In the case of the quinolinium derivatives possessing shorter alkyl substituent, the association to complex and NP were more separated (Fig. 2A). For the homologues with longer carbon chain, the association into NPs started at lower $[C_mC_1OQ^+]/[SCX4]$ mixing ratio and occurred in a wider range. The complexation was almost completely masked by NP formation for $C_{14}C_1OQ^+$ (Fig. 2C). The ΔH values at the plateau, which corresponded to the enthalpy change upon NP production, became more negative with the increase of the chain length. When $C_{10}C_1OQ^+$ was used as a titrant, the initial part of the enthalpogram could be fitted well assuming 1:1 binding and an association constant (K) of around $1.5 \times 10^5\ M^{-1}$ was obtained. This result fits to the tendency found for SCX4 complex formation of the smaller $C_mC_1OQ^+$ cations [24] ($m \leq 8$) where K varied from $4.6 \times 10^5\ M^{-1}$ to $2.1 \times 10^5\ M^{-1}$ upon increase of m from 1 to 8.

The larger SCX6 macrocycle induced similar association processes with the different 1-alkyl-6-alkoxy-quinoliniums (Figs. S3 and S4). The ΔH values of NP formations are summarized in Table 1. The alteration of the cavity size and the length of the alkoxy substituent of $C_1C_mOQ^+$ slightly influenced the exothermicity of NPs formation. In contrast, about 4.4- and 2.5-fold enthalpy gain enhancements were observed when the N-alkyl moiety of $C_mC_1OQ^+$ was varied from decyl to tetradecyl in the case of association with SCX4 and SCX6, respectively. In addition, longer alkyl group was necessary for NP formation when the hydrophobic carbon chain was attached to the heterocyclic nitrogen of the quinolinium ring instead of the oxygen at position 6. Our previous study demonstrated that both the quinolinium ring and the four first CH_2 groups linked to the heterocyclic nitrogen of $C_mC_1OQ^+$ guests are incorporated in SCX4 macrocycle upon 1:1 complexation [24]. In the case of $C_8C_1OQ^+$-SCX4, the fraction of the N-octyl moiety located outside the host is too short to induce NP formation. In contrast,

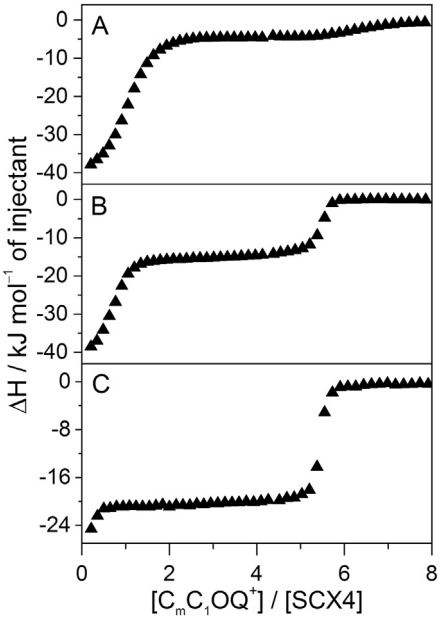

Fig. 2. Integrated heat evolved per injection (obtained after subtraction of the dilution heat to raw data) for the titration of 0.1 mM SCX4 with (A) 2 mM $C_{10}C_1OQ^+$, (B) 2 mM $C_{12}C_1OQ^+$, and (C) for the injection of 0.5 mM $C_{14}C_1OQ^+$ into 0.025 mM SCX4 solution.

Table 1
Effect of molecular structure variation on the enthalpy change of the formation of negatively charged NPs at 298 K.

		ΔH/kJ mol^{-1}			
Host	Guest	m = 8	m = 10	m = 12	m = 14
SCX4	$C_1C_mOQ^+$	−14.9	−16.7	[a]	
	$C_mC_1OQ^+$	[b]	−4.6	−15.2	−20.2
SCX6	$C_1C_mOQ^+$	−13.8	−18.0	[a]	
	$C_mC_1OQ^+$	[b]	−7.6	−15.1	−19.2

[a] Measurement cannot be performed because of the low solubility of the guest.
[b] NPs were not produced.

$C_1C_8OQ^+$-SCX4 complex initiates NP production in substantially exothermic process because the alkyl group connected via oxygen to the quinolinium ring protrudes from the SCX4 cavity [24]. Such a conformation permits efficient ordering of the alkyl chains and π-π interaction among the aromatic systems within the NPs. These effects also lead to much more negative ΔH for $C_1C_{10}OQ^+$-SCX4 NPs than for $C_{10}C_1OQ^+$-SCX4 NPs.

Surprisingly, despite its relatively short octyl group, $C_1C_8OQ^+$ aggregates both with SCX4 and with SCX6 into NP in more exothermic processes (Table 1) than 1-methyl-3-tetradecyl-imidazolium ($C_{14}mim^+$), which has a much longer hydrophobic tail. The enthalpy change upon formation of $C_{14}mim^+$-SCX4 and $C_{14}mim^+$-SCX6 NPs were found to be ΔH = −10.9 and − 10.8 kJ mol^{-1} in water at 298 K, respectively [16]. The substantial ΔH difference for the NPs of $C_1C_8OQ^+$ and $C_{14}mim^+$ suggests that the strength of the binding to the host and the interactions among the cationic headgroups of the amphiphiles significantly contribute to the stability of NPs. The more extended aromatic character of the quinolinium compared with imidazolium allows stronger π-π interaction with the benzene rings of SCXn as indicated by the more exothermic encapsulation of 6-methoxy-1-methylquinolinium [24] ($C_1C_1OQ^+$) in SCX4 (ΔH = −38.7 kJ mol^{-1}) and in SCX6 (ΔH = −32.1 kJ mol^{-1}) than the corresponding values obtained for 1,3-dimethylimidazolium inclusion [28] in SCX4 (ΔH = −29.2 kJ mol^{-1}) and in SCX6 (ΔH = −29.5 kJ mol^{-1}) in water at 298 K. In addition, the positive charge of the headgroup is more delocalized in quinolinium than in imidazolium. As a consequence, the repulsion among the cationic moieties is weaker within the NPs of $C_1C_mOQ^+$-SCXn types than within $C_{14}mim^+$-SCXn NPs.

3.3. Dynamic light scattering and zeta potential

To gain information on the size and charge of NPs, dynamic light scattering and zeta potential measurements were performed. Fig. 3 displays the results achieved upon addition of $C_{14}C_1OQ^+$ to SCX4 solutions. Negatively charged NPs were already produced at equimolar mixing ratio. Aggregation to larger particles took place when [$C_{14}C_1OQ^+$]/[SCX4] was around 5 and where the zeta potential changed from negative to positive. At even larger excess of $C_{14}C_1OQ^+$, SCX4 induced association into positively charged NPs. The mean diameters of the positive and negative NPs were around 80 and 45 nm, respectively. The positive NPs remained temporally more stable than the negatively charged NPs (Fig. S5).

The association of $C_{12}C_1OQ^+$ with SCX4 closely resembled that found for $C_{14}C_1OQ^+$ (Fig. S6), although larger NPs were produced and the positively charged NPs had smaller zeta potential. For both $C_{14}C_1OQ^+$ and $C_{12}C_1OQ^+$, the positive NPs had smaller mean diameter than the negative ones. This cannot be related to micelles in the suspension. At [$C_{14}C_1OQ^+$]/[SCX4] > 5, >95% of SCX4 was included in the NPs. As the stoichiometry in NPs was [$C_{14}C_1OQ^+$]/[SCX4] ≈ 5.5 (vide infra), the $C_{14}C_1OQ^+$ concentration in the solution remained below the cmc. The dynamic light scattering autocorrelation data (Fig. S7) also demonstrate only a single auto-correlation mode corresponding to NPs scattering and no indication is found for micelle formation.

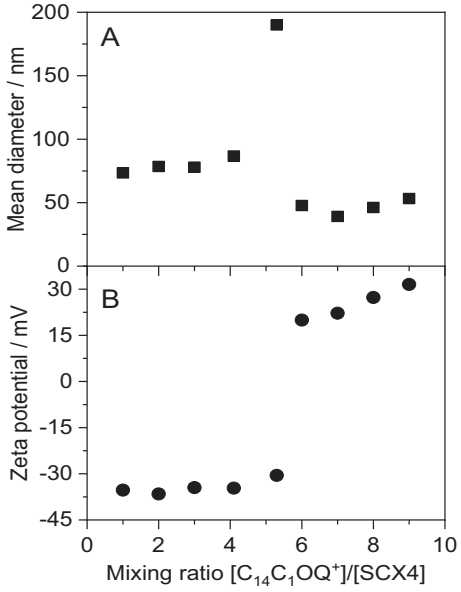

Fig. 3. (A) Mean diameter (■) and (B) zeta potential (●) of NPs as a function of mixing ratio [$C_{14}C_1OQ^+$]/[SCX4]. [SCX4] = 0.1 mM.

Further shortening of the N-alkyl substituent to decyl led to different behavior (Fig. 4). Namely, negatively charged NPs were formed up to [$C_{10}C_1OQ^+$]/[SCX4] = 11 mixing ratio, whereas coalescence occurred only at [$C_{10}C_1OQ^+$]/[SCX4] ≥ 12. The zeta potential progressively approached to zero when the relative amount of $C_{10}C_1OQ^+$ was raised in the solution. Positively charged NPs with a diameter larger than 350 nm appeared only at substantial (17–20-fold) quinolinium excess, but they were unstable and coalesced in less than 1 h. A similar behavior was observed with SCX6 and size and zeta potential of NPs formed between SCX6 and $C_mC_1OQ^+$ are given in Fig. S8.

With $C_1C_mOQ^+$ homologues, NP formation started already in the case of the octyl derivative and the characteristics of $C_1C_8OQ^+$-SCX4 NPs (Fig. S9) were similar to those of $C_{10}C_1OQ^+$-SCX4 NPs. Negative particles were formed up to [$C_1C_8OQ^+$]/[SCX4] = 8 mixing ratio. On

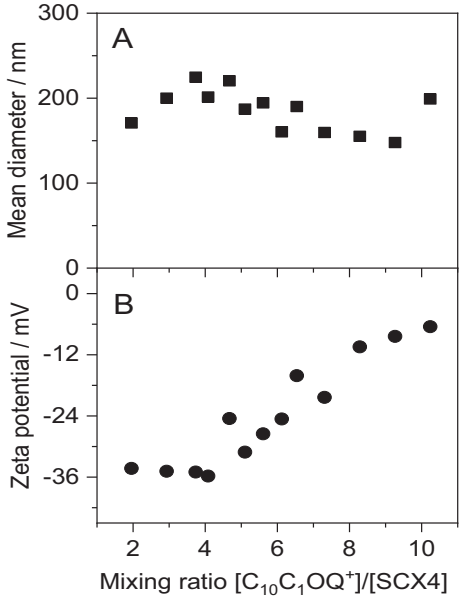

Fig. 4. Effect of [$C_{10}C_1OQ^+$]/[SCX4] mixing ratio variation on the (A) mean diameter and (B) zeta potential of NPs produced in 0.1 mM SCX4 solutions.

the other hand, the variation of mean diameter and zeta potential of $C_1C_{10}OQ^+$-SCX4 and $C_1C_{12}OQ^+$-SCX4 associates (Fig. S10) were alike that we observed for the NPs containing the long chain homologues of $C_mC_1OQ^+$ (m = 12 or 14). Fig. S11 shows the similar results obtained with SCX6.

3.4. Stoichiometry of the constituents in the NPs

The relative amounts of the constituents in the NPs were determined as a difference between the total concentrations and the concentrations in the liquid phase. After the separation of NPs by ultracentrifugation, the supernatants were analyzed by total carbon content measurements and the quinolinium amount was obtained by spectrophotometry [11]. Fig. 5 presents the $C_mC_1OQ^+$:SCXn molar ratio in the NPs as a function of the mixing ratio of the constituents. The $C_{14}C_1OQ^+$:SCX4 stoichiometry barely varied within the particles and the mean value was 5.5. The SCX4 percentage in the NPs rose up to a mixing ratio of 5. Above this value >95% of SCX4 was included in the NPs. On the other hand, >95% of $C_{14}C_1OQ^+$ was included in the NPs until the mixing ratio of 5, and then the excess amount of $C_{14}C_1OQ^+$ unbound in NPs increased. Anyhow, the $C_{14}C_1OQ^+$ concentration in the supernatant remained below the cmc even at high mixing ratios. The almost constant chemical composition of NPs ($C_{14}C_1OQ^+$:SCX4 = 5.5 and $C_{14}C_1OQ^+$:SCX6 = 7.2) was close to the charge compensation between the quinolinium cations and the polyanionic macrocycle. At pH 7, SCX4 had 5, whereas SCX6 had 8 negative charges because not only were the sulfonate groups deprotonated but also one or two phenolic OH group(s) released proton from the former and latter cavitands, respectively. The negative logarithms of the acid dissociation constants (pK_a) of the phenolic OH group is 3.2 in SCX4 whereas pK_a = 3.29, 4.91, and 12.5 values have been reported for SCX6. [25] At a mixing ratio below charge neutralization, the outer layer of the NPs was mainly composed of SCXn. Hence, negative zeta potential developed. When the abundance of $C_{14}C_1OQ^+$ exceeded the stoichiometry of charge compensation, the surface of NPs was predominantly covered by $C_{14}C_1OQ^+$ resulting in positive zeta potential.

$C_{12}C_1OQ^+$ produced NPs with stoichiometries almost independent of the mixing ratio similar to the findings with $C_{14}C_1OQ^+$. In contrast, the amount of $C_{10}C_1OQ^+$ relative to SCXn in the NPs strongly increased with the $C_{10}C_1OQ^+$:SCXn molar mixing ratio (Fig. 5). The stoichiometries in NPs were lower than those corresponding to the compensation of SCXn charges. This caused the negative zeta potential of NPs, which approached to zero at large $C_{10}C_1OQ^+$ excess (Fig. 4). The variation of NP stoichiometry with the mixing ratio may indicate that NPs are assembled by less cooperative interactions than in the case of $C_{14}C_1OQ^+$. This is corroborated by the fact that NP formation of $C_{10}C_1OQ^+$ has the smallest |ΔH| value (Table 1). As mentioned above, our previous study suggested that only part of the N-alkyl moiety is located outside the host for the 1:1 complexes of SCXn and $C_mC_1OQ^+$ with m > 4. The N-alkyl fraction outside the host was too short to induce NP formation for m = 8. The protruding part the alkyl chain outside the SCXn cavity grows with m allowing cooperative binding via hydrophobic and electrostatic interactions within NPs. When m = 10, the interactions are not strong enough to induce cooperative binding.

The stoichiometry of $C_1C_mOQ^+$-SCXn NPs did not show such a large variation with the mixing ratio as found for $C_{10}C_1OQ^+$-SCXn NPs. A small decrease of the stoichiometry was noticed only for $C_1C_8OQ^+$-SCXn NPs at low mixing ratios (Fig. S12). The insensitivity of the particle composition to the mixing ratio arises from the high binding affinity of $C_1C_mOQ^+$ to SCXn, which is demonstrated by the substantial ΔH gain upon association (Table 1). The nearly axial orientation of the alkyl chain in $C_1C_mOQ^+$-SCXn complexes minimizes the unfavorable contact with the host and promotes the assembly with several quinolinium cations. Thus, the stoichiometry corresponding to charge compensation is easily reached in the associates.

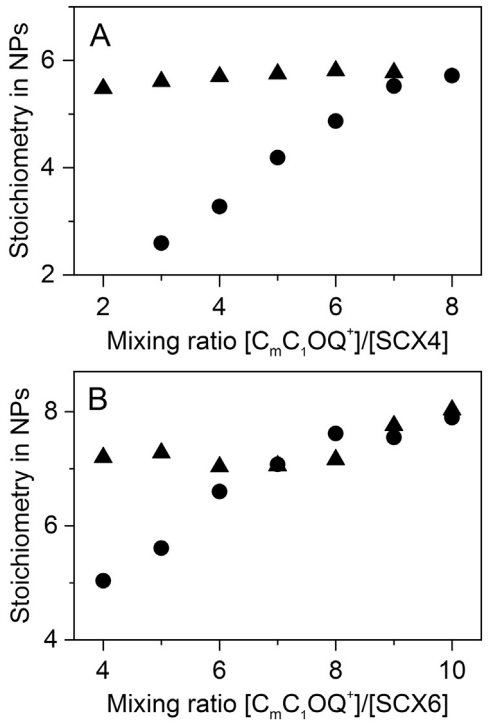

Fig. 5. $C_mC_1OQ^+$:SCXn molar ratio in the NPs as a function of the mixing ratio of the constituents using (A) SCX4 and (B) SCX6 macrocycles with $C_{10}C_1OQ^+$ (●) and $C_{14}C_1OQ^+$ (▲).

3.5. Morphology of nanoparticles

To reveal the shape and internal structure of NPs in their aqueous environment, cryogenic transmission electron microscopy (cryo-TEM) images were recorded after mixing the components at 296 K. Fig. 6 shows representative results for negatively and positively charged NPs taken after adding $C_{14}C_1OQ^+$ to SCX4 solution in molar ratio of 5 and 9, respectively. Both types of NPs appeared as well-separated uniformly dense spheres, as previously reported [15–17] for negative $C_{14}C_1OQ^+$-SCX6 NPs. The positive $C_{14}C_1OQ^+$-SCX6 NPs were also spherical, but some of them appeared as stacked circle planes (Fig. S13C, such structures have been reported for the NPs composed of $C_{14}mim^+$ and SCX6 [11]). Cryo-TEM images showed comparable particle size to the mean diameter determined by DLS measurements (Table S1). Dense spherical nanoparticles were also observed for other $C_mC_1OQ^+$-SCXn NPs and $C_1C_8OQ^+$-SCXn NPs at different molar mixing ratios (Fig. S14).

Interestingly, the positively charged $C_1C_{10}OQ^+$-SCXn and $C_1C_{12}OQ^+$-SCXn NPs provided entirely different images (Figs. 7–8, and Figs. S15–S17). They had non-spherical shape and internal structures showing equidistant lines about 3 nm apart in various areas of the nanoscale objects indicating periodic spacing of molecular layers. This regular spacing could correspond to the size of one self-assembled unit that is a SCXn decorated with as much $C_1C_{10}OQ^+$ or $C_1C_{12}OQ^+$ as necessary to ensure charge compensation.

The $C_1C_{10}OQ^+$-SCX4 NPs showed very well-defined structures with periodic spacing of molecular layers. Although the shape of NPs was not spherical, angular edges were noticed for most of them (Fig. S15). Many $C_1C_{10}OQ^+$-SCX6 NPs had a barrel-like appearance. They were partly aggregated and exhibited parallel lattice fringes (Fig. S16).The positively charged $C_1C_{12}OQ^+$-SCX4 NPs were inhomogeneous with a variety of profiles. A few of them exhibited empty space inside and nonuniform density. Aggregation and patterns like a fingerprint were also noticed (Fig. S17). In the case of $C_1C_{12}OQ^+$-SCX6, different types of organizations also coexisted. Nanoarchitectures of different shape, size and

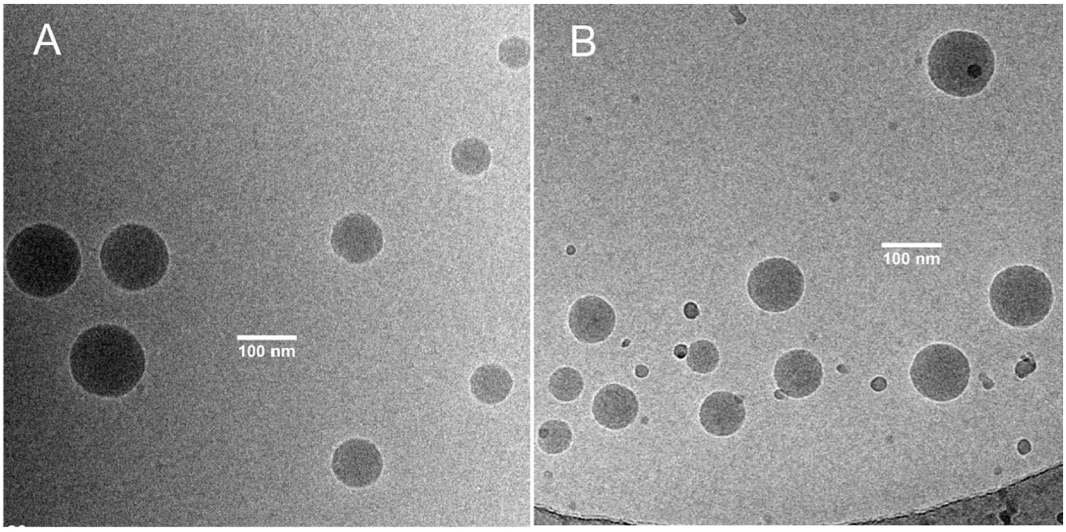

Fig. 6. Cryo-TEM images of NPs prepared from $C_{14}C_1OQ^+$ and SCX4 (0.2 mM) at mixing ratio (A) 5 and (B) 9.

contrast were observed. Some had a well-defined contour; others had a more diffuse border. The internal structure extended to different domains developing fingerprint-like pattern (Fig. S18).

4. Discussion

The location and length of the alkyl chain on the quinolinium are the determining parameters for the shape and internal structures of NPs. Unstructured and spherical NPs appear for $C_mC_1OQ^+$-SCXn, whereas structured architectures are produced for $C_1C_mOQ^+$-SCXn. Among the different nano-assemblies formed with SCXn [11,16–18], the ones obtained with $C_1C_mOQ^+$ ($m > 8$) were the first that led to non-spherical but structured aggregates. These structured morphologies remind the ones formed by nanoparticulate ordered mesophases of lipids, cubosomes or hexosomes [29,30]. In the present study, the nanoparticulate assemblies correspond to $C_1C_mOQ^+$-SCXn associates with precise stoichiometries (vide supra) and not to $C_1C_mOQ^+$ aqueous mesophases. Putaux and coworkers observed the self-assembly of β-cyclodextrins grafted with octyl or dodecyl groups into hexosomes [10]. When the total degree of substitution (TDS) of the cyclodextrin cavitand was >5, barrel-like assemblies with columnar inverse hexagonal structure (hexosomes) were produced, whereas spherical NPs with a multibilayer structure were created at TDS < 5.

The morphology differences between $C_mC_1OQ^+$-SCXn and $C_1C_mOQ^+$-SCXn may be attributed to conformational changes of SCXn upon association with one or the other type of amphiphile. Indeed, SCX6 is known to have a high molecular flexibility and can adopt several different conformations among which the double partial cone structure is the most probable [31,32]. SCX4 is more rigid and exist predominantly in cone conformation which undergoes ring inversion [33]. Despite the differences in the conformational mobility of SCX4 and SCX6, the NPs of both cavitands undergo a change from disordered nano-assemblies to structured aggregates when the nature of their amphiphile constituents is altered. This suggests that the structural features of NPs are probably controlled by the modification of the orientation of the amphiphilic guest in the host cavity and the conformational changes of the SCXn macrocycles play a less important role. The morphology of NPs composed of 1-alkyl-6-methoxy-quinolium-SCXn supramolecular amphiphile units also alters with the molecular structure of the constituents. Although each SCXn is surrounded by as much cationic amphiphiles as their total anionic charge (5 for SXC4 or 8 for SXC6), the organization of within these building blocks strongly depends on the location of the alkyl chain on the quinolinium moieties.

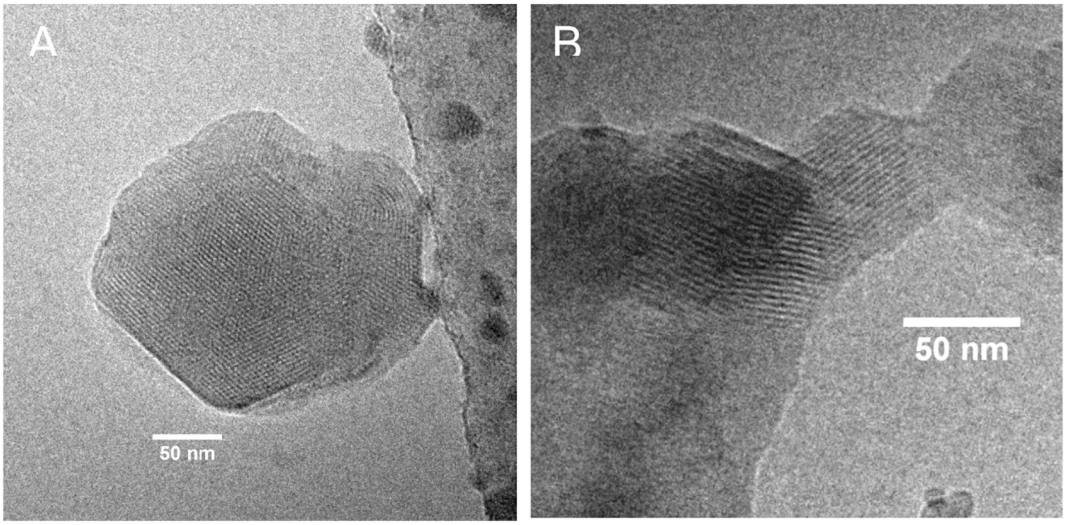

Fig. 7. Cryo-TEM images of positive NPs prepared from $C_1C_{10}OQ^+$ and (A) SCX4 (0.125 mM) or (B) SCX6 (0.1 mM) at mixing ratio 7 and 10, respectively.

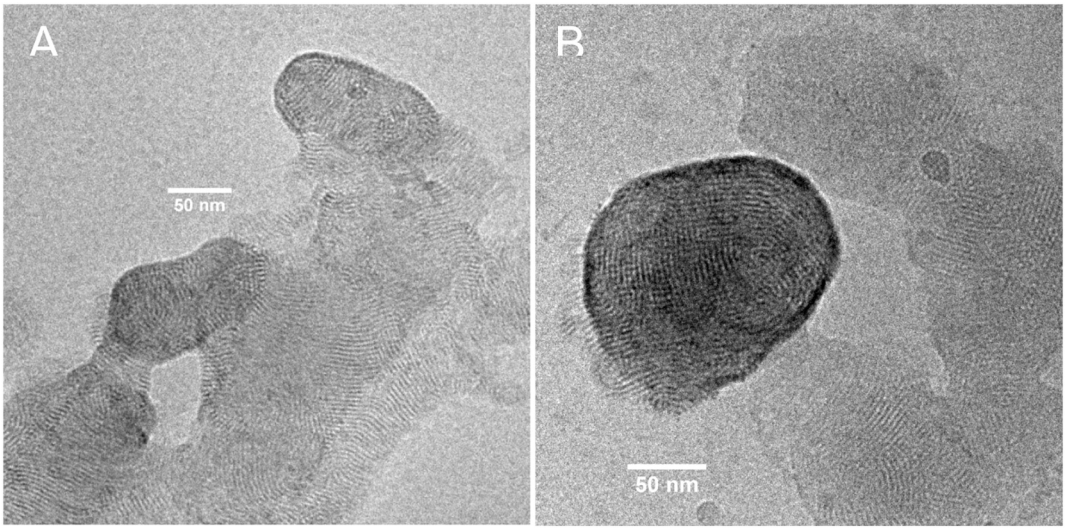

Fig. 8. Cryo-TEM images of positive NPs prepared from $C_1C_{12}OQ^+$ and (A) SCX4 (0.125 mM) or (B) SCX6 (0.1 mM) at mixing ratio 7 and 10, respectively.

When $C_mC_1OQ^+$ cations bind to SCXn, a few of the methylene groups close to the heterocyclic nitrogen are situated within the macrocycle whereas the alkyl substituents of other quinoliniums protrude from the cavity (Scheme 2A). Such ordering leads to looser interaction among the aliphatic chains which impedes the alignment of the $C_mC_1OQ^+$-SCXn units into layers. Therefore, the formation of spherical NPs without any regular inner structure becomes preferable.

In contrast, the alkoxy chains are oriented outward from the host macrocycle within $C_1C_mOQ^+$-SCXn segments which allows tighter interactions (Scheme 2B). Hence, these building elements can be arranged into lamellar structures. The $C_1C_mOQ^+$-SCXn associates are the supramolecular analogues of β-cyclodextrin grafted with alkyl groups (β-CD-C_n). In the former case, 5 or 8 alkoxy-substituted quinolinium cations are linked by electrostatic and hydrophobic interactions to SCX4 and SCX6, respectively, while 7 aliphatic chains are covalently attached to each macrocycle in β-CD-C_n. Due to the closely related structures of their building blocks, $C_1C_{10}OQ^+$-SCX4 and $C_1C_{12}OQ^+$-SCX4 NPs exhibited similar but less well defined morphology to those composed of β-CD-C_n molecules [10]. When SCX4 was replaced with SCX6, ultrastructuring and barrel-like arrangements were more clearly observed for $C_1C_{10}OQ^+$-SCX6 NPs. In some cases, crystal structures are organized in the three-dimensional space with planes intersecting at about 120° for NPs comprising SCX4 (Fig. 7A) or SCX6 (Fig. S18). This may indicate local hexagonal structure. We can infer from our cryo-TEM results that the self-assembly of $C_1C_mOQ^+$ with SCXn brings about nanoparticulate ordered mesophases. These kinds of structures have attracted considerable attention because of their large surface area and ability to solubilize both hydrophilic and hydrophobic compounds.

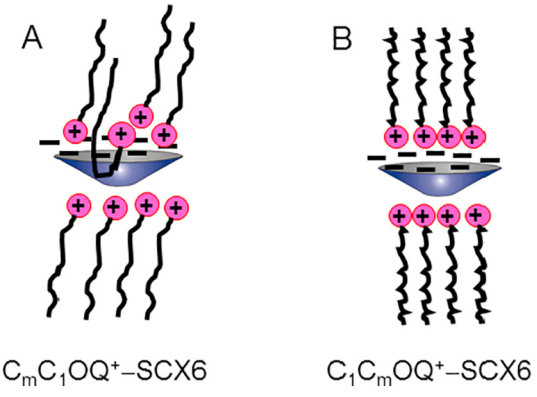

Scheme 2. Structure of substituted quinolium-SCX6 supramolecular amphiphiles

5. Conclusions

The association features of $C_1C_mOQ^+$ and $C_mC_1OQ^+$ considerably differ both in the presence and absence of SCXn cavitands. Only the latter type of amphiphiles is able to produce micelles. The micellization of $C_mC_1OQ^+Br^-$ homologues is exothermic if the 1-alkyl substituent is composed of at least 10 carbon atoms. The cmc diminishes about 17-fold when the 1-decyl substituent is changed to 1-tetradecyl. $C_1C_mOQ^+$ cations do not associate because their iodide salt has low solubility. However, even the octyl homologue of $C_1C_mOQ^+$ is capable of assembly with SCXn into nanoparticles because of the substantial enthalpy diminution of this process. The nearly axial outward orientation of the alkoxy group from the host interior facilitates the binding of as many $C_1C_mOQ^+$ cations as needed for the compensation of the SCXn charge. The building blocks produced thereby self-organize into mesophase domains, which are incorporated into NPs of irregular shape. In contrast, a part of the aliphatic moiety of SCXn-linked $C_mC_1OQ^+$ amphiphiles is included in the host. This impedes the ordering of the methylene chains into layers and the formation of spherical NPs without any regular inner structure becomes preferable. Because of the unfavorable direction of the alkyl group in $C_mC_1OQ^+$-SCXn, longer carbon chain is required for the aggregation into NPs than in the case of $C_1C_mOQ^+$-SCXn and the enthalpy change upon association alters to a larger extent with the increase of the number of methylene groups. The exothermicity and the mode of aggregation into NPs depends, to a great extent, on the orientation of the hydrophobic tail within the supramolecular amphiphile, but alteration of the macrocycle from SCX4 to SCX6 causes a minor effect. The morphologies obtained with $C_1C_mOQ^+$ constituents correspond to nanoparticulate ordered mesophases. Such structures attract widespread interest owing to their versatile potential applications.

Acknowledgement

This work was supported by the National Research, Development and Innovation Fund (NKFIH, Grant K123995), the BIONANO GINOP-2.3.2-15-2016-00017 project (to ZM and LB), and the János Bolyai Research Scholarship Program of the Hungarian Academy of Sciences (to ZM).

Declaration of competing interest

None.

Appendix A. Supplementary data

Supplementary data to this article can be found online at https://doi.org/10.1016/j.molliq.2019.111656.

References

[1] C. Stoffelen, J. Huskens, Soft supramolecular nanoparticles by noncovalent and host–guest interactions, Small 12 (2016) 96–119.
[2] H. Shelley, R.J. Babu, Role of cyclodextrins in nanoparticle-based drug delivery systems, J. Pharm. Sci. 107 (2018) 1741–1753.
[3] L. Jiang, Y. Yan, J. Huang, Versatility of cyclodextrins in self-assembly systems of amphiphiles, Adv. Colloid Interf. Sci. 169 (2011) 13–25.
[4] J. Zhang, X. Shen, Temperature-induced reversible transition between vesicle and supramolecular hydrogel in the aqueous ionic liquid−β-cyclodextrin system, J. Phys. Chem. B 117 (2013) 1451–1457.
[5] L. Jiang, M. Deng, Y. Wang, D. Liang, Y. Yan, J. Huang, Special effect of β-cyclodextrin on the aggregation behavior of mixed cationic/anionic surfactant systems, J. Phys. Chem. B 113 (2009) 7498–7504.
[6] G. Chen, M. Jiang, Cyclodextrin-based inclusion complexation bridging supramolecular chemistry and macromolecular self-assembly, Chem. Soc. Rev. 40 (2011) 2254–2266.
[7] Y. Chen, Y.-M. Zhang, Y. Liu, Multidimensional nanoarchitectures based on cyclodextrins, Chem. Commun. 46 (2010) 5622–5633.
[8] S. Engel, N. Möller, B.J. Ravoo, Stimulus-responsive assembly of nanoparticles using host–guest interactions of cyclodextrins, Chem. Eur. J. 24 (2018) 4741–4748.
[9] B. Jing, X. Chen, X. Wang, C. Yang, Y. Xie, H. Qiu, Self-assembly vesicles made from a cyclodextrin supramolecular complex, Chem. Eur. J. 13 (2007) 9137–9142.
[10] J.-L. Putaux, C. Lancelon-Pin, F.-X. Legrand, M. Pastrello, L. Choisnard, A. Gèze, C. Rochas, D. Wouessidjewe, Self-assembly of amphiphilic biotransesterified β-cyclodextrins: supramolecular structure of nanoparticles and surface properties, Langmuir 33 (2017) 7917–7928.
[11] V. Wintgens, C. Le Coeur, C. Amiel, J.M. Guigner, J.G. Harangozó, Z. Miskolczy, L. Biczók, 4-Sulfonatocalix[6]arene-induced aggregation of ionic liquids, Langmuir 29 (2013) 7682–7688.
[12] K. Wang, D.-S. Guo, M.-Y. Zhao, Y. Liu, A supramolecular vesicle based on the complexation of p-sulfonatocalixarene with protamine and its trypsin-triggered controllable-release properties, Chem. Eur. J. 22 (2016) 1475–1483.
[13] V. Francisco, N. Basilio, L. Garcia-Rio, J.R. Leis, E.F. Marques, C. Vazquez-Vazquez, Novel catanionic vesicles from calixarene and single-chain surfactant, Chem. Commun. 46 (2010) 6551–6553.
[14] P. Xing, T. Sun, A. Hao, Vesicles from supramolecular amphiphiles, RSC Adv. 3 (2013) 24776–24793.
[15] N. Basilio, D.A. Spudeit, J. Bastos, L. Scorsin, H.D. Fiedler, F. Nome, L. Garcia-Rio, Exploring the charged nature of supramolecular micelles based on p-sulfonatocalix[6]arene and dodecyltrimethylammonium bromide, Phys. Chem. Chem. Phys. 17 (2015) 26378–26385.
[16] J.G. Harangozó, V. Wintgens, Z. Miskolczy, J.-M. Guigner, C. Amiel, L. Biczók, Effect of macrocycle size on the self-assembly of methylimidazolium surfactant with sulfonatocalix[n]arenes, Langmuir 32 (2016) 10651–10658.
[17] V. Wintgens, J.G. Harangozó, Z. Miskolczy, J.-M. Guigner, C. Amiel, L. Biczók, Effect of headgroup variation on the self-assembly of cationic surfactants with sulfonatocalix[6]arene, Langmuir 33 (2017) 8052–8061.
[18] V. Wintgens, Z. Miskolczy, J.M. Guigner, C. Amiel, J.G. Harangozó, L. Biczók, Reversible manoparticle-micelle transformation of ionic liquid-sulfonatocalix[6]arene aggregates, Langmuir 31 (2015) 6655–6662.
[19] K. Wang, D.-S. Guo, X. Wang, Y. Liu, Multistimuli responsive supramolecular vesicles based on the recognition of p-sulfonatocalixarene and its controllable release of doxorubicin, ACS Nano 5 (2011) 2880–2894.
[20] K. Wang, D.-S. Guo, Y. Liu, Temperature-controlled supramolecular vesicles modulated by p-sulfonatocalix[5]arene with pyrene, Chem. Eur. J. 16 (2010) 8006–8011.
[21] D.-S. Guo, Y. Liu, Supramolecular chemistry of p-sulfonatocalix[n]arenes and its biological applications, Acc. Chem. Res. 47 (2014) 1925–1934.
[22] O. Danylyuk, K. Suwinska, Solid-state interactions of calixarenes with biorelevant molecules, Chem. Commun. (2009) 5799–5813.
[23] J.L. Atwood, L.J. Barbour, M.J. Hardie, C.L. Raston, Metal sulfonatocalix[4,5]arene complexes: bi-layers, capsules, spheres, tubular arrays and beyond, Coord. Chem. Rev. 222 (2001) 3–32.
[24] V. Wintgens, C. Lorthioir, Z. Miskolczy, C. Amiel, L. Biczók, Substituent effects on the inclusion of 1-alkyl-6-alkoxy-quinolinium in 4-sulfonatocalix[n]arenes, ACS Omega 3 (2018) 8631–8637.
[25] K. Suga, T. Ohzono, M. Negishi, K. Deuchi, Y. Morita, Effect of various cations on the acidity of p-sulfonatocalixarenes, Supramol. Sci. 5 (1998) 9–14.
[26] R.J. Meagher, T.A. Hatton, A. Bose, Enthalpy measurements in aqueous SDS/DTAB solutions using isothermal titration microcalorimetry, Langmuir 14 (1998) 4081–4087.
[27] S. Paula, W. Sues, J. Tuchtenhagen, A. Blume, Thermodynamics of micelle formation as a function of temperature: a high sensitivity titration calorimetry study, J. Phys. Chem. 99 (1995) 11742–11751.
[28] V. Wintgens, L. Biczók, Z. Miskolczy, Thermodynamics of host-guest complexation between p-sulfonatocalixarenes and 1-alkyl-3-methylimidazolium type ionic liquids, Thermochim. Acta 523 (2011) 227–231.
[29] B.J. Boyd, D.V. Whittaker, S.-M. Khoo, G. Davey, Hexosomes formed from glycerate surfactants—formulation as a colloidal carrier for irinotecan, Int. J. Pharm. 318 (2006) 154–162.
[30] H.M.G. Barriga, M.N. Holme, M.M. Stevens, Cubosomes: the next generation of smart lipid nanoparticles? Angew. Chem. Int. Ed. 58 (2019) 2958–2978.
[31] F. Perret, A.N. Lazar, A.W. Coleman, Biochemistry of the para-sulfonato-calix[n]arenes, Chem. Commun. (2006) 2425–2438.
[32] J.L. Atwood, D.L. Clark, R.K. Juneja, G.W. Orr, K.D. Robinson, R.L. Vincent, Double partial cone conformation for Na_8{calix[6]arene sulfonate}·20.5H_2O and its parent acid, J. Am. Chem. Soc. 114 (1992) 7558–7559.
[33] Y. Israëli, C. Detellier, Ring inversion kinetics of p-sulfonatocalix[4]arene and of its Ca(II) and La(III) complexes in water and water-acetone solutions, Phys. Chem. Chem. Phys. 6 (2004) 1253–1257.